X-ray Waveguide Mode in Resonance with a Periodic Structure

K. Okamoto,[1] T. Noma,[2] A. Komoto,[1] W. Kubo,[1] M. Takahashi,[1] A. Iida,[3] and H. Miyata[1,*]

[1]*Frontier Research Center, Canon Inc., 3-30-2 Shimomaruko, Ohta-ku, Tokyo 146-8501, Japan*
[2]*Nanomaterials R&D Center, Canon Inc., 3-30-2 Shimomaruko, Ohta-ku, Tokyo 146-8501, Japan*
[3]*Photon Factory, High Energy Accelerator Research Organization, 1-1 O-ho, Tsukuba, Ibaraki 305-0801, Japan*

(Received 2 April 2012; published 5 December 2012)

We present a novel concept for x-ray waveguiding based on electromagnetism in photonic crystals, using a waveguide consisting of a pair of claddings sandwiching a core with a periodic structure. By confining the x rays undergoing multiple interference in the core by total reflection, a characteristic waveguide mode whose field distribution matches the periodicity of the core is formed. The distinctively low propagation loss enables the single-mode propagation of x rays. This concept opens broad application possibilities in x-ray physics from coherent imaging to x-ray quantum optics.

DOI: 10.1103/PhysRevLett.109.233907 PACS numbers: 42.70.Qs, 41.50.+h, 42.25.Kb, 42.79.Gn

With the recent success of the free electron laser [1], x-ray beams with unprecedented coherency have been realized and are expected to be a great tool to unveil many unresolved matters in various fields of science. Such highly coherent and collimated x-ray beams are increasing their importance in analytical and diagnostic applications, such as x-ray imaging. The devices that enable the coherence control of x rays will bring significant advancement in x-ray optics. Spiller and Segmüller [2] proposed the concept of an x-ray waveguide (WG) and demonstrated the selective propagation of x rays on individual discrete modes using a planar WG. Thin films [3,4] and air gaps [5–7] have been used for the planar WGs' core where x ray is one-dimensionally confined, and characteristic behaviors of x rays, such as coherent propagation, and consequent formation of a fine x-ray beam have been reported. For advanced control of x rays, WGs with much sophisticated structures have been studied [8,9]. Salditt and coworkers expanded the concept of the planar WGs to two dimensions to achieve an x-ray point source [10] and a microprobe [11–13] for various applications [14–17]. However, regardless of the dimension, the cross section of the core in the conventional WGs must be extremely small due to the restriction by the single-mode condition [18], in order to realize the spatially coherent x rays. This limits the x-ray flux through the WGs and leads to undesired large divergence of the emitting beams. Although the integration [9,19] of multiple single-mode WGs can increase the total size of the core cross section, totally coherent guided x rays cannot be achieved, because the guided x rays in each WG do not interfere with each other. Very recently, Bukreeva *et al.* proposed an x-ray WG having a wide core, which enables a coherent propagation of x rays by selecting a high-order WG mode using the claddings periodically formed in the guiding direction [20].

Here we report a novel single-mode x-ray WG based on physics of photonic crystals [21] in the x-ray regime. Figure 1 shows the concept of the WG that realizes the coherent propagation on a selected WG mode. The multiple interference of x rays in a periodic structure causes a specific propagation mode that is resonant with the periodicity. Confining the x rays of this mode within the core consisting of a periodic multilayer by total reflection (TR) at the core-cladding interfaces allows the formation of a unique high-order WG mode. This periodicity-resonant WG (PRWG) mode, which is resonant with both the total thickness and the periodicity of the core, enables the low-loss coherent propagation of x rays. In this letter, the concept of the novel guiding of x rays as well as the formation of a beam with "high quality," that is, improved coherency and a narrow divergence, is demonstrated using a WG consisting of a B_4C/Al_2O_3 multilayer core sandwiched by W claddings. In addition to the usefulness of the emitted unique x rays from this PRWG to practical applications such as imaging and analysis, this PRWG will be applied to new fields of x-ray physics including x-ray quantum optics [22,23].

The physics of photonic crystals is valid even in the x-ray regime where the refractive index n of a material is defined as $n = 1 - \delta - i\beta = n' - i\beta$, where n' and β represent the real and the imaginary part, respectively. In a 1D periodic structure with enough numbers of pairs of layers with different n', multiple reflection and refraction of x rays cause multiple interference as shown in the right part of Fig. 1, which forms photonic bands (PBs) in the dispersion relation between the frequency ω and the wave vector $\boldsymbol{k} = (k_y, k_z)$ [24]. In Fig. 1, n'_{high} and n'_{low} are the

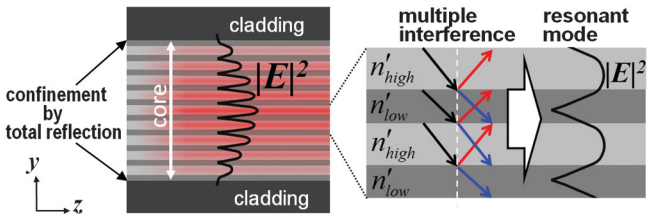

FIG. 1 (color). Concept of the periodicity-resonant waveguide.

higher and the lower real parts of refractive indices, respectively. In particular ranges of k_z, there exist PB gaps, which cause Bragg reflections. Since the most resonant mode in the PB structure corresponds to the edge of the doubly degenerate lowest band, it has the symmetric wave vectors $\boldsymbol{k} = (\pm k_y, k_z)$, where $\mathrm{Re}[k_y]$ is $\pi/(n'_{\mathrm{eff}}a)$ with a period of a and an effective refractive index of n'_{eff}. The field profile of this resonant mode has the fine fringes with the same periodicity as that of the periodic structure, and the antinodes are located in the layers with higher n' (smaller β), as shown in Fig. 1. When the claddings are formed to confine the x rays of this resonant mode in the core consisting of a finite multilayer by TR, the PRWG mode, which is resonant with both the periodicity and the total width of the core, is formed, as shown in the left part of Fig. 1. Because of the fine fringe pattern of the field distribution as described above, the PRWG mode achieves a low propagation loss.

We define the effective propagation angle θ_{eff} of the WG modes with respect to the z direction as Eq. (1),

$$\theta_{\mathrm{eff}} = \cos^{-1}\frac{\mathrm{Re}[k_z]}{|\boldsymbol{k}_0|}. \tag{1}$$

Here, $\boldsymbol{k}_0$ is the wave vector in vacuum and k_z is equivalent to the propagation constant of the WG modes. Multiple interference needs to occur to have the PRWG mode spatially coherent over the entire core area along the y axis, which requires the following condition:

$$\theta_{C\_\mathrm{in}} < \theta_B \sim \theta_{\mathrm{eff}}. \tag{2}$$

Here, θ_{C_in} is the critical angle for TR at the interfaces of the adjacent layers in the multilayer core and θ_B is the Bragg angle corresponding to the center of the PB gap, which is close to θ_{eff} of the PRWG mode. When this condition is not satisfied, the x rays are confined in each layer with high n', and consequently, multiple interference does not take place. In addition, Eq. (3) must be satisfied to confine the x rays on the PRWG mode by TR. Here, $\theta_{C\_\mathrm{total}}$ is the critical angle for TR at the core-cladding interfaces,

$$\theta_B < \theta_{C\_\mathrm{total}}. \tag{3}$$

Under these conditions, we need to know the envelope of the field in the core with a periodicity for the complete description of the PRWG mode. Considering the confinement by TR, the field distribution of the PRWG mode is estimated using the coupled wave theory [25] by assuming the two incident x rays R_+ and R_- into the core from the two opposed core-cladding interfaces. The periodic index modulation causes the diffracted x rays $S_\pm$. Now we define the coupling coefficient κ between $R_\pm$ and $S_\pm$ as Eq. (4), when the refractive index $n(y, z)$ is expressed by Eq. (5) as the summation of the averaged constant $(n'_{\mathrm{avg}}, \beta_{\mathrm{avg}})$ and the sinusoidal perturbation of (n'_1, β_1). Here, $K = 2\pi/a$,

$$\kappa = \frac{\pi}{\lambda}n'_1 - i\frac{1}{2}\beta_1, \tag{4}$$

$$n(y,z) = [n'_{\mathrm{avg}} + n'_1\cos(Ky)] - i[\beta_{\mathrm{avg}} + \beta_1\cos(Ky)]. \tag{5}$$

The total field distribution $E(\boldsymbol{r}) \equiv E(y, z)$ can be expressed with Eqs. (6)–(8) derived from the coupled wave theory [25],

$$E(\boldsymbol{r}) = R_+e^{-i\boldsymbol{k}_{R_+}\cdot\boldsymbol{r}} + S_+e^{-i(\boldsymbol{k}_{R_+}-\boldsymbol{G})\cdot\boldsymbol{r}} + R_-e^{-i\boldsymbol{k}_{R_-}\cdot\boldsymbol{r}} + S_-e^{-i(\boldsymbol{k}_{R_-}+\boldsymbol{G})\cdot\boldsymbol{r}}, \tag{6}$$

$$R_\pm = \frac{\Gamma_1 e^{\gamma_1 y \pm \gamma_2(L/2)} - \Gamma_2 e^{\gamma_2 y \pm \gamma_1(L/2)}}{\Gamma_1 e^{\mp(\gamma_1-\gamma_2)(L/2)} - \Gamma_2 e^{\pm(\gamma_1-\gamma_2)(L/2)}}, \tag{7a}$$

$$S_\pm = -i\kappa\frac{e^{\gamma_1 y \pm \gamma_2(L/2)} - e^{\gamma_2 y \pm \gamma_1(L/2)}}{\Gamma_1 e^{\mp(\gamma_1-\gamma_2)(L/2)} - \Gamma_2 e^{\pm(\gamma_1-\gamma_2)(L/2)}}, \tag{7b}$$

$$\Gamma_{1,2} = \left(\sin\theta_{\mathrm{in}} - \frac{K}{k}\right)\gamma_{1,2} + \beta_{\mathrm{avg}} + i\vartheta. \tag{8}$$

In these equations, $\boldsymbol{k}_{R_\pm} = (\pm k\sin\theta_{\mathrm{in}}, k\cos\theta_{\mathrm{in}})$ are the wave vectors of the x rays with the incident angle with respect to the z direction of θ_{in}, $\boldsymbol{G} = (K, 0)$ is the reciprocal lattice vector of the periodic structure, $k = 2\pi n'_{\mathrm{avg}}/\lambda$ is the wave number for the x rays in the core with an averaged index, L is the core width, and $\vartheta = \Delta\theta K\sin\theta_B$ is a dephasing from the Bragg condition, where $\Delta\theta = \theta_{\mathrm{in}} - \theta_B$ and $\theta_B = \sin^{-1}(K/2k)$. The envelope of the intensity distribution of the electric field in the core, $|E|^2_{\mathrm{env}}$, is expressed as

$$|E|^2_{\mathrm{env}} = |R_+|^2 + |S_+|^2 + |R_-|^2 + |S_-|^2. \tag{9}$$

Figure 2 shows the dependence of $|E|^2_{\mathrm{env}}$ on the normalized propagation angle, $\Delta\theta/\theta_B$, along the y axis, calculated using Eqs. (4)–(9) for the x rays with a photon energy of 10 keV. The core has a periodic structure with the following parameters: $a = 15$ nm, $L = 1.5$ μm, $n'_{\mathrm{avg}} = 0.99999458$, $n'_1 = 5.32\times10^{-7}$, $\beta_{\mathrm{avg}} = 2.42\times10^{-8}$,

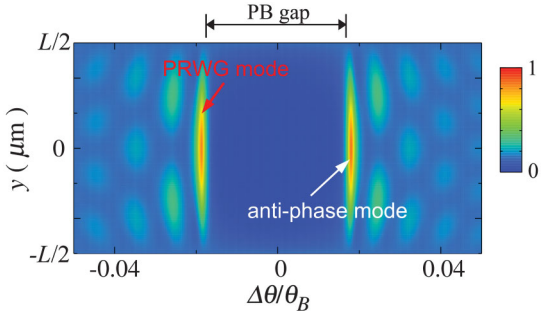

FIG. 2 (color). Dependence of the envelope of the electric field intensity distribution in the multilayer core, $|E|^2_{\mathrm{env}}$ (arb.units), on the normalized propagation angle $\Delta\theta/\theta_B$.

and $\beta_1 = 2.09 \times 10^{-8}$. As shown in Fig. 2, a PB gap is formed at a range of $|\Delta\theta/\theta_B| \leq \sim 0.018$, and the WG modes are formed outside of that. The red arrow indicates the $|E|^2_{env}$ of the PRWG mode, which is formed at a propagation angle corresponding to the PB edge just below the PB gap. It is also shown that the electric field of the PRWG mode is concentrated in the center of the core, which helps lowering the level of the evanescent field in the claddings. This field concentration is caused by the distributed feedback effect enhanced by the confinement. Although the antiphase mode (white arrow in Fig. 2) has an equivalent envelope, its propagation loss is large because the antinodes of the fringes of the field distribution are located in the regions with large β. It should be noted that the propagation loss is not taken into account in Fig. 2. The other modes are resonant only with the total width of the core. The above theoretical discussion clarifies that the PRWG mode, which is formed through the strong distributed feedback effect, is highly selective in spite of its extraordinary high order.

The theoretical prediction is confirmed by the numerical eigenmode calculation by the finite element method (FEM) for the transverse electric WG modes (x-ray energy = 10 keV). The WG in the calculation consists of a core and two W claddings with a thickness of 200 nm sandwiching the core. The core is a multilayer with a period of 15 nm, consisting of the alternative stacking of 100 pairs of B_4C and Al_2O_3 layers with a thickness of 12 nm and 3 nm, respectively. Figure 3(a) shows the linear attenuation coefficient μ corresponding to the WG modes with the effective propagation angle θ_{eff}. μ means the propagation loss, which is related to the propagation constant k_z, as $\mu = 2\,\mathrm{Im}[k_z]$. The μ of the PRWG mode is distinctively small compared to the other modes (less than 1/2), while that of the antiphase mode is the largest. To clarify the reason for the low propagation loss, the field distribution of the PRWG mode along the y axis is calculated, as shown in Figs. 3(b) and 3(c). Figure 3(b) proves that $|E|^2$ concentrates in the center of the core, which lowers the loss through the reduction of the evanescent tails in the claddings. Figure 3(c) shows the distribution of the real amplitude of the electric field, Re[E], in a narrower y region. It is confirmed from this figure that the periodicity of the fringes matches that of the core, and the antinodes are located in the B_4C layers with small β (white area), which also contributes to the low propagation loss. As described above, the PRWG mode becomes dominant compared to the other ones, which are attenuated faster. In this way, the single-mode x-ray propagation on this PRWG mode is realized and the guided x rays become spatially coherent over the entire width of the core of ~ 1.5 μm. The coherency and the fine periodic fringes in the field distribution lead to the formation of an x-ray beam with a small divergence angle ($< 0.01°$).

We experimentally demonstrated the selective propagation of x rays on the PRWG mode and the consequent formation of an x-ray beam with improved spatial coherency. The experimental setup is shown in Fig. 4(a). The structure of the WG is substantially the same as that used for the calculation. An B_4C/Al_2O_3 multilayer was formed on a 20 nm bottom W cladding on a silicon substrate by alternative sputtering, and the top W cladding was formed thereon. The number of the pairs is 100, and B_4C contacts

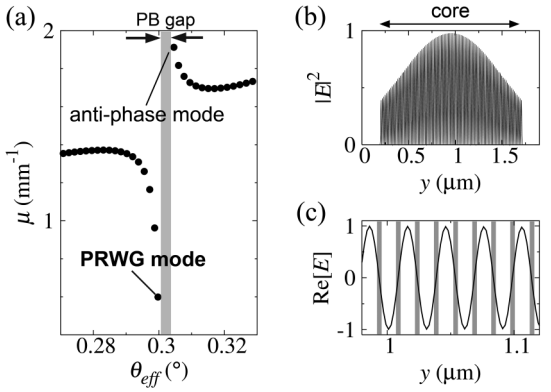

FIG. 3. FEM calculation results for the transverse electric WG modes. (a) Linear attenuation coefficient μ corresponding to the WG modes with the effective propagation angle θ_{eff}. (b) Distribution of the electric field intensity $|E|^2$ of the PRWG mode along the y axis. (c) Distribution of the real amplitude of the field Re[E] of the PRWG mode in a narrower y region. The gray and the white areas correspond to the Al_2O_3 and B_4C layers, respectively. $|E|^2$ and Re[E] are normalized by each maximum.

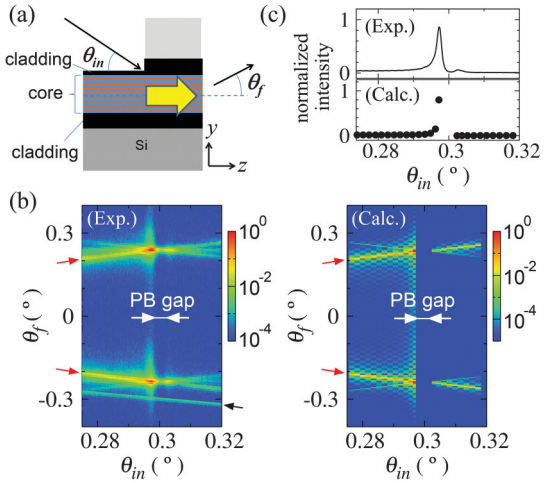

FIG. 4 (color). (a) Experimental setup. (b) The incident angle dependence of the far-field patterns: experiment (left) and calculation (right). The line indicated by a black arrow is caused by a scarcely refracted transmission of the third diffraction component from the monochromator. In the calculations, the resonant angles are estimated by the transfer matrix method for the WG modes obtained from the FEM eigenmode calculations. (c) Dependence of the x-ray intensity on θ_{in}, along the zeroth-order line in (b) (normalized with the maximum value).

to each cladding. The materials forming the multilayer were selected by taking the following three requirements into account: large contrast of n', small β, and good quality of the film. The roughness at the interfaces of the multilayer, which seriously deteriorates the WG performance for rms > 1 nm, was reduced to the level of rms < 0.2 nm. The thickness of each layer, 12 nm for B_4C and 3 nm for Al_2O_3, was determined to maximize the calculated transmittance. The WG consists of two parts: the coupling region with the thin top W cladding (2 nm) and the WG region with the thicker one (20 nm). The experiments were conducted using synchrotron radiation with 10 keV at the PF BL-4A, KEK, Japan. The monochromated x rays using a Si(111) double crystal monochromator were shaped to a beam with 150 μm height (y) and 1000 μm width (x) by a 4-jaw slit. The divergence angle and the energy band width $\Delta E/E$ of the beam are $\sim 0.002°$ and $\sim 2 \times 10^{-4}$, respectively. The x-ray beam was impinged to the coupling region at a grazing angle θ_{in} with respect to the z axis in the y-z plane, and the far-field patterns (spatial intensity distribution) were recorded by a Pilatus 2D detector (Dectris Ltd.) with changing θ_{in}. The emission angle θ_f as well as the divergence angle of the beam was estimated from the obtained patterns and the distance between the detector and the WG end. The WG was mounted on a goniometer, which enables the precise control of rotation and translation. The length of the WG region was 2.5 mm, and a lead glass plate was fixed on the top cladding to block the specular reflection. The impinged x rays couple to a WG mode via the evanescent field when θ_{in} matches its θ_{eff}.

The incident angle dependence of the experimentally obtained and the calculated far-field patterns are shown in Fig. 4(b). The formation of a PB gap at $\theta_{\text{in}} \sim 0.3°$ is confirmed in each image. The symmetric two bright lines with respect to $\theta_f = 0°$ (red arrows) are caused by the zeroth-order Fraunhofer diffraction originating from the near-field distribution of the WG modes. The points with high intensity at an incident angle just below the PB gap correspond to the PRWG mode. The divergence of the emitted x-ray beam is $\sim 0.009°$. Figure 4(c) shows the intensity profile along the zeroth-order diffraction line. The intensity of the x rays propagated on the PRWG mode is about an order of magnitude higher than those on the other modes. Thus, the selective propagation of x rays on the PRWG mode and the consequent formation of a beam with a small divergence are experimentally confirmed.

In conclusion, we demonstrated the coherent propagation of x rays by selecting a single high-order PRWG mode, which is caused by the strong resonance effect with a periodic structure enhanced by the confinement. Actually, this WG works as a filter, which extracts the coherent component in the original x-ray beam. The new WG based on a concept of photonic crystals in this paper will find various applications in analysis, diagnosis, and quantum optics using the unique features of the x rays with outstanding spatial coherency. The concept in this paper can be extended to structures with 2D and 3D periodicity, which enables more sophisticated control of x rays.

The authors acknowledge R. Sekiguchi and T. Ouchi for fruitful discussions and kind reviewing. This work was performed in a joint collaboration between Photon Factory and Canon Inc. (Proposal No. 2010C011).

*miyata.hirokatsu@canon.co.jp

[1] P. Emma *et al.*, Nat. Photonics **4**, 641 (2010).
[2] E. Spiller and A. Segmüller, Appl. Phys. Lett. **24**, 60 (1974).
[3] Y. P. Feng, S. K. Sinha, H. W. Deckman, J. B. Hastings, and D. P. Siddons, Phys. Rev. Lett. **71**, 537 (1993).
[4] S. Lagomarsino, W. Jark, S. D. Fonzo, A. Cedola, B. Mueller, P. Engstrom, and C. Riekel, J. Appl. Phys. **79**, 4471 (1996).
[5] M. J. Zwanenburg, J. F. Peters, J. H. H. Bongaerts, S. A. de Vries, D. L. Abernathy, and J. F. van der Veen, Phys. Rev. Lett. **82**, 1696 (1999).
[6] C. Bergemann, H. Keymeulen, and J. F. van der Veen, Phys. Rev. Lett. **91**, 204801 (2003).
[7] I. Bukreeva, A. Popov, D. Pelliccia, A. Cedola, S. B. Dabagov, and S. Lagomarsino, Phys. Rev. Lett. **97**, 184801 (2006).
[8] T. Salditt, S. P. Krüger, C. Fuhse, and C. Bähtz, Phys. Rev. Lett. **100**, 184801 (2008).
[9] F. Pfeiffer, T. Salditt, P. Høghøj, I. Anderson, and N. Schell, Phys. Rev. B **62**, 16 939 (2000).
[10] F. Pfeiffer, C. David, M. Burghammer, C. Riekel, and T. Salditt, Science **297**, 230 (2002).
[11] A. Jarre, C. Fuhse, C. Ollinger, J. Seeger, R. Tucoulou, and T. Salditt, Phys. Rev. Lett. **94**, 074801 (2005).
[12] A. Jarre, J. Seeger, C. Ollinger, C. Fuhse, C. David, and T. Salditt, J. Appl. Phys. **101**, 054306 (2007).
[13] A. Kohlstedt, S. Kalbfleisch, T. Salditt, M. Reiche, U. Gösele, E. Lima, and P. Willmott, Appl. Phys. A **91**, 7 (2008).
[14] T. H. Metzger, Science **297**, 205 (2002).
[15] C. Ollinger, C. Fuhse, S. Kalbfleisch, R. Tucoulou, and T. Salditt, Appl. Phys. Lett. **91**, 051110 (2007).
[16] K. Giewekemeyer, S. P. Krüger, S. Kalbfleisch, M. Bartels, C. Beta, and T. Salditt, Phys. Rev. A **83**, 023804 (2011).
[17] C. Fuhse, C. Ollinger, and T. Salditt, Phys. Rev. Lett. **97**, 254801 (2006).
[18] C. Fuhse and T. Salditt, Opt. Commun. **265**, 140 (2006).
[19] C. Ollinger, C. Fuhse, A. Jarre, and T. Salditt, Physica (Amsterdam) **357**, 53 (2005).
[20] I. Bukreeva, A. Cedola, A. Sorrentino, D. Pelliccia, V. Asadchikov, and S. Lagomarsino, Opt. Lett. **36**, 2602 (2011).
[21] E. Yablonovitch, Phys. Rev. Lett. **58**, 2059 (1987).
[22] R. Röhlsberger, K. Schlage, B. Sahoo, S. Couet, and R. Rüffer, Science **328**, 1248 (2010).
[23] R. Röhlsberger, H.-C. Wille, K. Schlarge, and B. Sahoo, Nature (London) **482**, 199 (2012).
[24] J. D. Joannopoulos, S. G. Johnson, J. N. Winn, and R. D. Meade, *Photonic Crystals: Molding the Flow of Light* (Princeton University Press, Princeton, NJ, 2008), 2nd ed.
[25] H. Kogelnik, Bell Syst. Tech. J. **48**, 2909 (1969).